




RESEARCH ARTICLE | MARCH 17 2020

Piezoelectric biaxial strain effects on the optical and photoluminescence spectra of 2D III–VI compound α -In₂Se₃ nanosheets

Feng Guo ; Yongxin Lyu; Michal Bartłomiej Jedrzejczyk; Yuqian Zhao; Weng Fu lo; Gongxun Bai; Wenzhuo Wu ; Jianhua Hao  



Appl. Phys. Lett. 116, 113101 (2020)

<https://doi.org/10.1063/5.0001795>

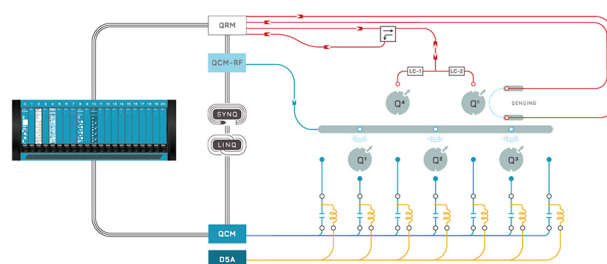


CrossMark



Integrates all
Instrumentation + Software
for Control and Readout of

**Superconducting Qubits
NV-Centers
Spin Qubits**



Spin Qubits Setup

[find out more >](#)

Piezoelectric biaxial strain effects on the optical and photoluminescence spectra of 2D III–VI compound α - In_2Se_3 nanosheets

Cite as: Appl. Phys. Lett. **116**, 113101 (2020); doi: [10.1063/5.0001795](https://doi.org/10.1063/5.0001795)

Submitted: 20 January 2020 · Accepted: 8 March 2020 ·

Published Online: 17 March 2020



View Online



Export Citation



CrossMark

Feng Guo,¹ Yongxin Lyu,¹ Michal Bartłomiej Jędrzejczyk,¹ Yuqian Zhao,¹ Weng Fu Io,¹ Gongxun Bai,² Wenzhuo Wu,³ and Jianhua Hao^{1,a)}

AFFILIATIONS

¹Department of Applied Physics, The Hong Kong Polytechnic University, Hong Kong 999077, People's Republic of China

²Institute of Optoelectronic Materials and Devices, China Jiliang University, Hangzhou 310018, People's Republic of China

³School of Industrial Engineering, Purdue University, West Lafayette, Indiana 47907, USA

^{a)}Author to whom correspondence should be addressed: apjhao@polyu.edu.hk

ABSTRACT

The controllable biaxial strain is experimentally imposed on α - In_2Se_3 nanosheets by an electromechanical device. A redshift of Raman spectra is observed from the nanosheets under the strain. The Grüneisen parameter is calculated to analyze the strain effect on the vibrational behavior. Photoluminescence shows a blueshift, which can reach up to 215 meV per 1% strain. Such tunability of optical characteristics observed from α - In_2Se_3 nanosheets is much higher than that from conventional semiconductors. The physical mechanism behind the observation is investigated, which is related to the variations in the energy band and photoexcited carriers under a piezoelectric field and laser power.

Published under license by AIP Publishing. <https://doi.org/10.1063/5.0001795>

Two-dimensional (2D) optoelectronic devices, such as nano-laser devices, light emitting diodes, and photodetectors, have been continuously developed due to their unique physical properties.^{1–3} In order to meet the demands of technological progress, substantial efforts have been devoted to the dynamic tuning of the band structure of materials. Strain engineering is a promising strategy to promote the performance of next-generation optoelectronic devices due to its cost effective and straightforward manufacturing process.^{4–7} In addition, strain engineering provides an excellent platform to probe and modulate the optical and electrical transport properties of optoelectronic materials. Particularly, applying strain often gives rise to unexpected effects on 2D materials due to the ultrathin layered structures of 2D compounds. For example, in order to realize the potential application of graphene with the absence of bandgap, strain engineering has been used to open a tiny bandgap in its Brillouin zone.^{8,9} Specifically, a variety of 2D piezoelectric materials, such as MoS_2 and WS_2 , have been highly investigated for the effects of strain on optical and vibrational properties, and most of the studies attribute the change in the energy band to strain.^{10,11} However, the relevant strain effects on the optical properties of the III–VI layered semiconductor as an important group of 2D materials still remain unexplored. Thus, it is highly desirable to explore

the strain engineering of emerging 2D piezoelectric materials that allow further understanding of the underlying mechanism. Recently, III–VI compound α - In_2Se_3 has been verified to be a layered van der Waals 2D material with a bandgap of ~ 1.4 eV and superior piezoelectric and ferroelectric properties, which leads to potential applications for photodetectors and infrared LEDs.^{12–14} However, until now, there are a few reports on modulating the optical and luminescence properties of α - In_2Se_3 by applying strain dynamically.

Generally, there are two methods to impose strain on 2D materials. The first one is to impose uniaxial strain through stretching or bending the flexible substrates, such as PDMS, PMMA, and PET. The other way is to place 2D materials on a piezoelectric substrate to induce a biaxial strain. Compared with uniaxial strain imposed by mechanically bending a flexible substrate, biaxial strain can be modulated more precisely, ascribed to its control by applied voltage. Hence, the single crystalline $(1-x)[\text{Pb}(\text{Mg}_{1/3}\text{Nb}_{2/3})\text{O}_3]-x[\text{PbTiO}_3]$ (PMN-PT) was adopted in this work as the piezoelectric substrate due to its superior electromechanical and converse piezoelectric properties, which is extensively used in our previous studies.^{15–19} In this work, the Raman and photoluminescence (PL) spectra of mechanically exfoliated layered α - In_2Se_3 nanosheets under biaxial strain triggered by the

PMN-PT (001) substrate have been studied, which provides an effective method to modulate and investigate 2D material properties via an *in situ* and dynamical approach.

α -In₂Se₃ nanosheets were prepared through mechanical exfoliation from the bulk crystal, which was purchased from 2D semiconductor Co. Prior to the transfer process, a 100 nm-thick Au layer was coated on the backside of the substrate as a bottom electrode, while the Pt film with 20 nm thickness was sputtered on the polished side of the substrate as a top electrode. The overall resistance of metal Au and Pt electrodes is only several ohms, which is much smaller than that of the insulating PMN-PT dielectric substrate (\sim G Ω). Hence, the majority of the bias voltage was dropped on the substrate. The schematic diagram of Raman and PL measurements is shown in Fig. 1(a). The thickness of the nanosheet was measured to be about 30 nm using an Asylum MFP 3D Infinity atomic force microscope (AFM) under tapping mode as shown in Fig. 1(b). To observe the optical properties and vibrational behavior, the Raman and PL spectra were characterized by a WITec_Confocal Raman system using a laser as an excitation source with a spot size of 1 μ m and a wavelength of 532 nm. In order to avoid destroying the sample, smaller laser power less than 0.5 mW was used in our experiment. The bias voltage was supplied using a Keithley 2410 Source Meter. Prior to the measurements, an electric field (E) of 10 kV/cm was applied on the PMN-PT substrate for polarization.

Raman peaks were found to locate at 89, 104, 180, and 196 cm^{-1} according to the report,²⁰ while four remarkable peaks at 90, 104, 180, and 195 cm^{-1} were revealed by Xue *et al.*²¹ To examine the vibrational behavior of α -In₂Se₃ on the PMN-PT substrate, the Raman spectrum was measured as shown in the inset of Fig. 2(a). The Raman peaks are centered at \sim 88, 104, 180, and 194 cm^{-1} , which correspond to the phonon modes of α -In₂Se₃. The strongest peak located at 104 cm^{-1} can be identified as the characteristic peak, which is attributed to A(LO+TO) phonon modes.²¹ Therefore, the strongest A(LO+TO) phonon mode will be taken as a reference measured on the samples under low laser power excitation in the following measurements [inset of Fig. 2(b)].

Here, we define applying a positive voltage on the top of the substrate (the polished side with Pt) as a positive sign. According to the previous study, a compressive strain can be produced by a negative or positive bias voltage with a slope of -0.04% strain per 100 V.²² As shown in Fig. 2(a), with an increase in applied voltage from 0 to 500 V, the A(LO+TO) phonon mode shifts toward higher frequency, while a similar trend is observed when a negative voltage is applied. The relationship between the Raman shift and strain remains approximately linear at a rate of about $3.1 \text{ cm}^{-1}/\%$ for positive voltage. The shift of

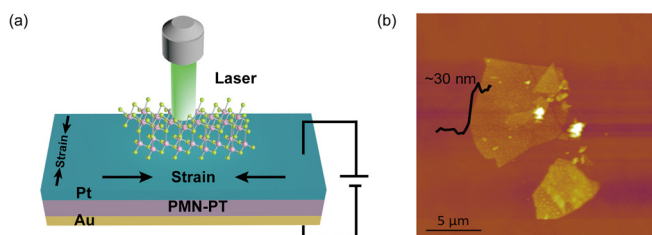


FIG. 1. (a) Schematic diagram of Raman and PL measurements via an electromechanical device (b) AFM image of α -In₂Se₃ nanosheets.

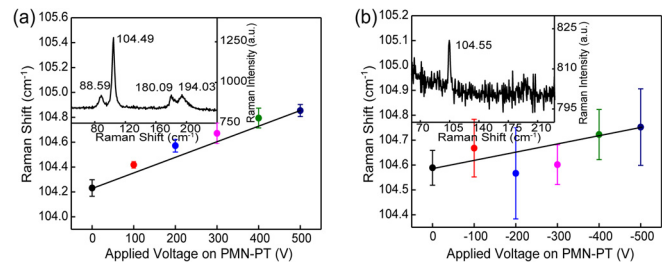


FIG. 2. The Raman peak position as a function of the applied voltage from (a) 0 to 500 V and (b) 0 to -500 V. Insets show the Raman spectrum of α -In₂Se₃ and the A(LO+TO) phonon mode, respectively.

the Raman peak is highly indicative of the variation in the lattice constant and vibrational behavior of phonons, which is commonly observed when strain is imposed on 2D materials.^{10,11} The Grüneisen parameter is an effective quantity to describe the rate of phonon frequency variations with respect to strain. It can be defined as follows:

$$\gamma = \frac{-1}{2\omega_0} \frac{\partial \omega}{\partial \varepsilon}, \quad (1)$$

where ω_0 and ω are Raman frequencies under no strain and finite biaxial strain, respectively, and ε is the biaxial strain applied on α -In₂Se₃. In this case, it can be simplified as

$$\gamma = -\frac{\Delta \omega}{2\omega_0 \varepsilon}. \quad (2)$$

Herein, the obtained Grüneisen parameters are 1.5 and 0.4 for the positive and negative voltages, respectively. However, the deformation of the piezoelectric PMN-PT substrate may not have been completely transferred onto the top α -In₂Se₃ layer because of the loss mainly at the interface. With the reference to the calibration where graphene was placed on PMN-PT in our previous work, the actual strain applied to the 2D material is about -0.011% per 100 V.²³ Assuming that the strain can be completely transferred to α -In₂Se₃ through the Pt layer for an ideal case, the actual Grüneisen parameters are 5.4 and 1.44, respectively. The Grüneisen parameter of the negative voltage case is slightly smaller than that of positive voltage. This may be attributed to a slight slippage during the process of applying strain. In other words, the data derived from the positive voltage case demonstrate the modulation ability of strain on the Raman frequency more comprehensively. Comparing our result with the reported Grüneisen parameters for graphene (1.4 under high pressure²⁴ and 1.99 under uniaxial strain²⁵) and MoS₂ (1.1 under uniaxial tensile mechanical strain¹⁰), piezoelectric substrate-induced biaxial strain can provide a more powerful tool to modulate and investigate the lattice vibration.

In order to investigate the evolution of the electronic structure in layered α -In₂Se₃ nanosheets under biaxial strain, the PL spectra were measured and normalized using their respective maximum values. As shown in Fig. 3(a), a PL peak located at 833.5 nm was observed in the samples under zero bias after polarization with 0.1 mW laser power. With an increase in positive voltage, the PL peak shows a blueshift remarkably, and the overall variation can reach up to 6.6 nm (11.87 meV). Similarly, Fig. 3(b) exhibits a linear decrease in the PL wavelength from 831.6 to 826.3 nm as the negative voltage varies from 0 to -500 V. The inset shows the PL emitting-wavelength as a

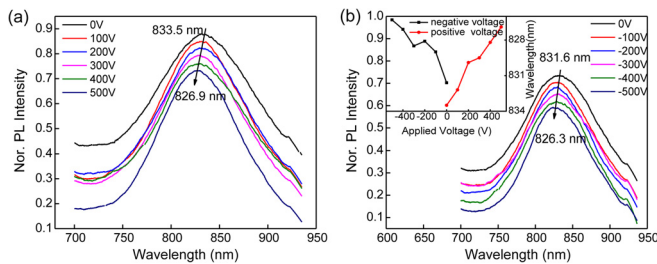


FIG. 3. PL spectra under various applied voltages from (a) 0 V to 500 V and (b) 0 V to -500 V with 0.1 mW laser power. The inset shows the PL peak position as a function of applied voltage from -500 V to 500 V.

function of applied voltage on the PMN-PT substrate, which indicates that the behavior of the PL peak shift is similar under positive and negative voltages due to voltage-driven piezoelectric induced biaxial compressive strain. It is worth noting that the tunability of the blueshift in the PL peak can approach to 215.82 meV/% under strain. Importantly, this value measured from the α -In₂Se₃ nanosheets is much larger than the magnitude of tunability observed in conventional semiconductors at nanoscale, as shown in Table I.

In general, the applied strain could result in the variation of bandgap in semiconductors, and the imposed electric field might play an important role as well. For example, a bandgap open of ~ 200 meV was observed in graphene under an electric field of 1 V/nm.²⁹ Here, in order to rule out the influence of the electric field on α -In₂Se₃ in the above measurements, we adopted a careful design of the α -In₂Se₃/Pt/

TABLE I. Effect of strain on the PL shift of α -In₂Se₃ and conventional semiconductors.

	Tunability of PL by strain (meV/%)	References
ZnO nanowire	~ 8.5	26
Silicon nanowire	~ 100	27
GaAs/AlGaAs quantum dots	~ 70	28
α -In ₂ Se ₃ nanosheets	215.82	This work

PMN-PT/Au structure. In this configuration, the electric field was merely imposed on the Pt/PMN-PT/Au structure, and there was no applied electric field through the α -In₂Se₃ nanosheets. Therefore, the applied electric field had little influence on the variation of bandgap. Noted that the strain could also induce a piezoelectric field in α -In₂Se₃, detailed discussions about the relationships between the electric field from piezoelectric and bandgap will be shown in the following parts.

Figure 4 displays the evolution of PL peaks as a function of laser power under different polarization and electric field conditions. As shown in Fig. 4(a), before the substrate is polarized, nanosheets exhibit a slight blueshift with increasing laser power. The phenomenon can be attributed to the Burstein Moss effect, which is commonly observed in a semiconductor with narrow bandgap.³⁰ After polarization, the emergence of a redshift from 833 to 836 nm can be seen in Fig. 4(b) as the laser power increases from 0.1 to 0.5 mW. The behavior is similar to the case of the electric field applied on the PMN-PT substrate. Although no voltage is applied on the substrate, there is some biaxial

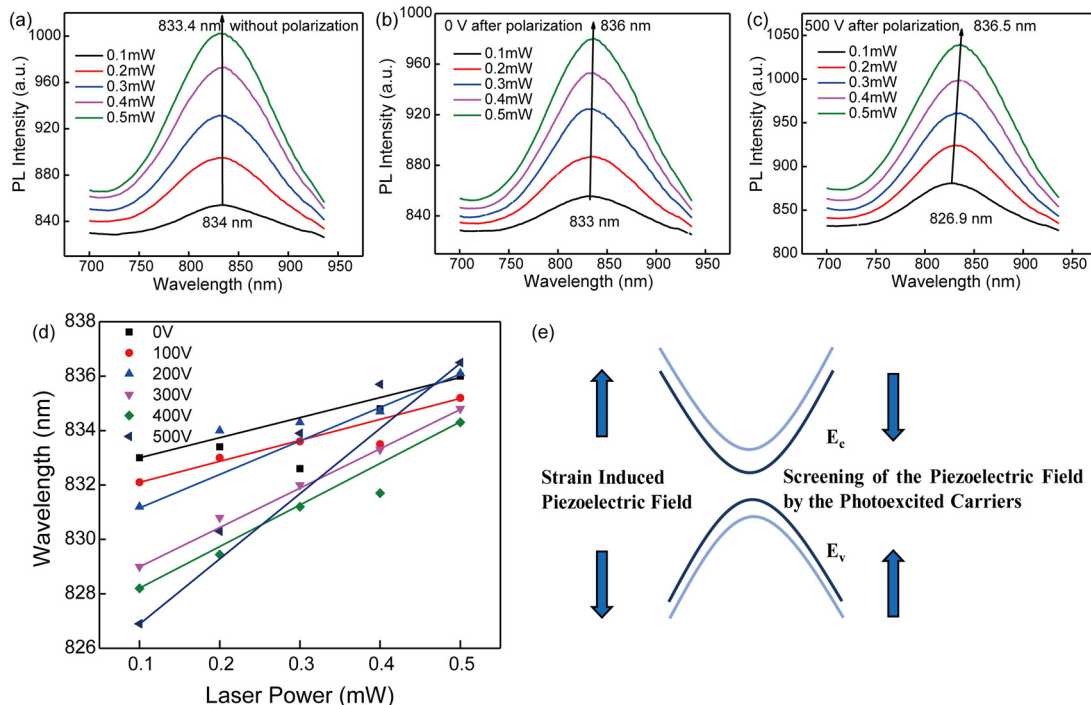


FIG. 4. PL spectra under various laser powers (a) before polarization, (b) 0 V after polarization, and (c) 500 V after polarization. (d) PL peak position as a function of laser power at various applied voltages. (e) Schematic energy band structure under piezoelectric fields and laser powers.

strain induced by the remanent polarization (P_r). Here, we take a positive voltage case as an example. With the increase in applied voltage from 0 to 500 V, the variation of the redshift becomes larger and larger under a laser power from 0.1 to 0.5 mW. Clearly, when the applied voltage was increased to 500 V, the laser power-dependent redshift significantly occurred from 826.9 to 836.5 nm as shown in Fig. 4(c).

The dependence of the PL redshift on laser power clearly evidences the effect of the piezoelectric field on α -In₂Se₃ bandgap. Logically, there are two factors that can influence the bandgap of nanosheets, namely, biaxial compressive strain and strain induced piezoelectric field. Considering a certain electric field applied on the PMN-PT substrate, the induced strain on α -In₂Se₃ remains unchanged regardless of the incident laser intensity. However, when increasing laser power, we observed a gradual shifting of the PL peak toward the wavelength for the fully relaxed nanosheet case in Fig. 4(d). Hence, speculation can be drawn that the tuning of α -In₂Se₃ bandgap is not induced by the biaxial compressive strain in a direct manner. As a matter of fact, this typical behavior is existed in the piezoelectric nanostructured material. The PL peak shift can be attributed to the screening of the piezoelectric field by the photoexcited carriers, and the analysis of excitation power dependent PL spectra is a common way to determine the relationship between the piezoelectric effect and bandgap variation of a piezoelectric material, such as GaN self-assembled quantum dots on AlN,³¹ InAs quantum dots grown on GaAs substrates,³² and InGaN quantum wells.³³ An experimental study has verified the co-existence of out-of-plane and in-plane piezoelectricity in α -In₂Se₃ due to its non-centrosymmetric structure.¹³ In this work, two different sources of the electric field may exist in the nanosheets, including the piezoelectric field and built-in electric field induced by the Pt/ α -In₂Se₃ Schottky junction. Since the Schottky contact built-in potential remains unchanged under varying strains, the only factor influencing the PL peak shift is the piezoelectric field. The charge density n induced by polarization can be calculated as follows:

$$n = \frac{2dY\varepsilon}{e}, \quad (3)$$

where d is the piezoelectric constant, Y is the Young's modulus, ε is the strain, and e is the elementary electric charge. According to the references, $d_{33} = 5.6$ pC/N,¹³ $d_{11} = 2.55$ pC/N³⁴ and $Y_{001} = 36.47$ GPa, $Y_{100} = 105.48$ GPa.³⁵ Assuming that the volume of the α -In₂Se₃ unit cell is a constant, when a strain of -0.055% is imposed in-plane under 500 V, a strain of 0.11% along the c -axis is induced simultaneously. As a result, the polarization induced charge concentration is $2.8 \times 10^{13} \text{ cm}^{-2}$ and $1.8 \times 10^{13} \text{ cm}^{-2}$ along in plane and out of plane directions, respectively.

In order to understand the effect of photoexcited carriers on the piezoelectric field, a semi-quantitative estimation of the number of electron-hole (e - h) pairs present in α -In₂Se₃ is performed when considering a laser power of 0.5 mW. The absorption of α -In₂Se₃ is $\sim 60\%$,³⁶ and the lifetime of e - h pair is ~ 70 ms.³⁷ Here, we assume that each photon absorbed by the nanosheet generates an e - h pair. Therefore, the photoexcited carriers with much higher charge density are derived compared with the polarization induced charge concentration on the order of 10^{22} cm^{-2} . The above calculation demonstrates that the photoexcited carriers are capable of effectively screening the strain-induced piezoelectric field. In practice, the quantum yield cannot reach up to 100%, and the Schottky contact-induced space charge

can also recombine with photoexcited carriers. Therefore, the blueshift of the PL peak with increasing voltage originates from the strain-induced piezoelectric field, and the laser power dependent redshift implies that the effect of the piezoelectric field on α -In₂Se₃ bandgap could be eliminated effectively by photoexcited carriers as shown in Fig. 4(e).

In conclusion, we have demonstrated the high tunability of α -In₂Se₃ Raman spectra and PL characteristics under compressive biaxial strain induced by the piezoelectric PMN-PT substrate. By precisely *in situ* modulating bias voltage on the substrate, the biaxial strain can be generated and delivered to α -In₂Se₃ nanosheets, resulting in the prominent shift in Raman and PL spectra. The vibrational behavior of α -In₂Se₃ is examined based on the Grüneisen parameter. In addition, the influence of the strain-induced piezoelectric field on the α -In₂Se₃ energy band is discussed, and we attribute the laser power dependent PL shift to the screening of the piezoelectric field by photoexcited e - h pairs. The method used in this work allows us to investigate in detail the effects induced by the piezoelectric PMN-PT substrate on the electronic structure and optical characteristics of 2D III-VI compound materials and may be extended to study other strain dependent phenomena, such as electricity and magnetism.

This work was supported by the Research Grant Council (RGC) of Hong Kong (RGC GRF No. PolyU 153023/18P).

REFERENCES

- ¹O. Salehzadeh, M. Djavid, N. H. Tran, I. Shih, and Z. Mi, *Nano Lett.* **15**, 5302 (2015).
- ²X. Wang and F. Xia, *Nat. Mater.* **14**, 264 (2015).
- ³Z. Yang, W. Jie, C. H. Mak, S. Lin, H. Lin, X. Yang, F. Yan, S. P. Lau, and J. Hao, *ACS Nano* **11**, 4225 (2017).
- ⁴W. Wu and Z. Wang, *Nat. Rev. Mater.* **1**, 16031 (2016).
- ⁵W. Wu, L. Wang, R. Yu, Y. Liu, S. H. Wei, J. Hone, and Z. Wang, *Adv. Mater.* **28**, 8463 (2016).
- ⁶M. O. Lipinski, H. Schuler, O. G. Schmidt, and K. Eberl, *Appl. Phys. Lett.* **77**, 1789 (2000).
- ⁷L. Seravalli, M. Minelli, P. Frigeri, P. Allegri, V. Avanzini, and S. Franchi, *Appl. Phys. Lett.* **82**, 2341 (2003).
- ⁸S.-M. Choi, S.-H. Jhi, and Y.-W. Son, *Phys. Rev. B* **81**, 081407(R) (2010).
- ⁹Z. Ni, T. Yu, Y. Lu, Y. Wang, Y. Feng, and Z. Shen, *ACS Nano* **2**, 2301 (2008).
- ¹⁰H. J. Conley, B. Wang, J. I. Ziegler, R. F. Haglund, Jr., S. T. Pantelides, and K. I. Bolotin, *Nano Lett.* **13**, 3626 (2013).
- ¹¹Y. Wang, C. Cong, W. Yang, J. Shang, N. Peimyoo, Y. Chen, J. Kang, J. Wang, W. Huang, and T. Yu, *Nano Res.* **8**, 2562 (2015).
- ¹²W. Ding, J. Zhu, Z. Wang, Y. Gao, D. Xiao, Y. Gu, Z. Zhang, and W. Zhu, *Nat. Commun.* **8**, 14956 (2017).
- ¹³F. Xue, J. Zhang, W. Hu, W. T. Hsu, A. Han, S. F. Leung, J. K. Huang, Y. Wan, S. Liu, J. Zhang, J. H. He, W. H. Chang, Z. L. Wang, X. Zhang, and L. J. Li, *ACS Nano* **12**, 4976 (2018).
- ¹⁴Y. Zhou, D. Wu, Y. Zhu, Y. Cho, Q. He, X. Yang, K. Herrera, Z. Chu, Y. Han, M. C. Downer, H. Peng, and K. Lai, *Nano Lett.* **17**, 5508 (2017).
- ¹⁵W. Jie, Y. Y. Hui, N. Y. Chan, Y. Zhang, S. P. Lau, and J. Hao, *J. Phys. Chem. C* **117**, 13747 (2013).
- ¹⁶Y. Zhang, G. Gao, H. L. W. Chan, J. Dai, Y. Wang, and J. Hao, *Adv. Mater.* **24**, 1729 (2012).
- ¹⁷L. Chen, M. C. Wong, G. Bai, W. Jie, and J. Hao, *Nano Energy* **14**, 372 (2015).
- ¹⁸Y. Zhang, W. Jie, P. Chen, W. Liu, and J. Hao, *Adv. Mater.* **30**, 1707007 (2018).
- ¹⁹G. Bai, Y. Zhang, and J. Hao, *Sci. Rep.* **4**, 5724 (2015).
- ²⁰S. Wan, Y. Li, W. Li, X. Mao, W. Zhu, and H. Zeng, *Nanoscale* **10**, 14885 (2018).
- ²¹F. Xue, W. Hu, K.-C. Lee, L.-S. Lu, J. Zhang, H.-L. Tang, A. Han, W.-T. Hsu, S. Tu, W. H. Chang, C.-H. Lien, J.-H. He, Z. Zhang, L.-J. Li, and X. Zhang, *Adv. Funct. Mater.* **28**, 1803738 (2018).

- ²²Y. Hui, X. Liu, W. Jie, N. Y. Chan, J. Hao, Y.-T. Hsu, L.-J. Li, W. Guo, and S. P. Lau, *ACS Nano* **7**, 7126 (2013).
- ²³W. Jie, Y. Y. Hui, Y. Zhang, S. P. Lau, and J. Hao, *Appl. Phys. Lett.* **102**, 223112 (2013).
- ²⁴M. Hanfland, H. Beister, and K. Syassen, *Phys. Rev. B* **39**, 12598 (1989).
- ²⁵T. M. G. Mohiuddin, A. Lombardo, R. R. Nair, A. Bonetti, G. Savini, R. Jalil, N. Bonini, D. M. Basko, C. Galiotis, N. Marzari, K. S. Novoselov, A. K. Geim, and A. C. Ferrari, *Phys. Rev. B* **79**, 205433 (2009).
- ²⁶R. W. Shao, K. Zheng, B. Wei, Y. F. Zhang, Y. J. Li, X. D. Han, Z. Zhang, and J. Zou, *Nanoscale* **6**, 4936 (2014).
- ²⁷D. Shiri, Y. Kong, A. Buin, and M. P. Anantram, *Appl. Phys. Lett.* **93**, 073114 (2008).
- ²⁸A. Rastelli, F. Ding, J. D. Plümhof, S. Kumar, R. Trotta, C. Deneke, A. Malachias, P. Atkinson, E. Zallo, T. Zander, A. Herklotz, R. Singh, V. Krápek, J. R. Schröter, S. Kiravittaya, M. Benyoucef, R. Hafenbrak, K. D. Jöns, D. J. Thurmer, D. Grimm, G. Bester, K. Dörr, P. Michler, and O. G. Schmidt, *Phys. Status Solidi B* **249**, 687 (2012).
- ²⁹K. F. Mak, C. H. Lui, J. Shan, and T. F. Heinz, *Phys. Rev. Lett.* **102**, 256405 (2009).
- ³⁰X. Liu, Q. Zhang, J. N. Yip, Q. Xiong, and T. C. Sum, *Nano Lett.* **13**, 5336 (2013).
- ³¹F. Widmann, J. Simon, B. Daudin, G. Feuillet, J. L. Rouvière, and N. T. Pelekanos, *Phys. Rev. B* **58**, R15989(R) (1998).
- ³²S. Sanguinetti, M. Gurioli, E. Grilli, M. Guzzi, and M. Henini, *Appl. Phys. Lett.* **77**, 1982 (2000).
- ³³H. Gotoh, T. Tawara, Y. Kobayashi, N. Kobayashi, and T. Saitoh, *Appl. Phys. Lett.* **83**, 4791 (2003).
- ³⁴L. Hu and X. Huang, *RSC Adv.* **7**, 55034 (2017).
- ³⁵N. D. Raranskii, V. N. Balazyuk, Z. D. Kovalyuk, N. I. Mel'nik, and V. B. Gevik, *Inorg. Mater.* **47**, 1174 (2011).
- ³⁶C. Julien, M. Eddrief, K. Kambas, and M. Balkanski, *Thin Solid Films* **137**, 27 (1986).
- ³⁷R. B. Jacobs-Gedrim, M. Shanmugam, N. Jain, C. A. Durcan, M. T. Murphy, T. M. Murray, R. J. Matyi, R. L. Moore, and B. Yu, *ACS Nano* **8**, 514 (2014).